J Nanopart Res (2014) 16:2689
DOI 10.1007/s11051-014-2689-3

RESEARCH PAPER

Doping effects on the structural, magnetic, and hyperfine properties of Gd-doped SnO_2 nanoparticles

H. Coelho-Júnior · J. C. R. Aquino · F. H. Aragón · P. Hidalgo · R. Cohen · L. C. C. M. Nagamine · J. A. H. Coaquira · S. W. da Silva · H. F. Brito

Received: 28 May 2014 / Accepted: 1 October 2014 / Published online: 23 December 2014

Abstract In this work we present the study of the structural, magnetic, and hyperfine properties of Gd-doped SnO_2 nanoparticles synthesized by a polymer precursor method. The X-ray diffraction data analysis shows the formation of the rutile-type structure in all samples with Gd content from 1.0 to 10.0 mol%. The mean crystallite size is $\sim$11 nm for the 1.0 mol% Gd-doped samples and it shows a decreasing tendency as the Gd content is increased. The analysis of magnetic measurements indicates the coexistence of ferromagnetic and paramagnetic phases for the 1.0 mol% Gd-doped sample; however, above that content, only a paramagnetic phase is observed. The ferromagnetic phase observed in the 1.0 mol% Gd-doped sample has been assigned to the presence of bound magnetic polarons which overlap to create a spin-split impurity band. Room-temperature ^{119}Sn Mössbauer measurements reveal the occurrence of strong electric quadrupole interactions. It has been determined that the absence of magnetic interactions even for 1.0 mol% Gd-doped sample has been related to the weak magnetic field associated to the exchange interaction between magnetic ions and the donor impurity band. The broad distribution of electric quadrupole interactions are attributed to the several non-equivalent surroundings of Sn^{4+} ions provoked by the entrance of Gd^{3+} ions and to the likely presence of Sn^{2+} ions. The isomer shift seems to be nearly independent of the Gd content for samples with Gd content below 7.5 mol%.

Keywords Gd-doped SnO_2 nanoparticles · Magnetic properties · Structural properties · Mössbauer spectroscopy · Spintronics

H. Coelho-Júnior · J. C. R. Aquino · F. H. Aragón · J. A. H. Coaquira (✉) · S. W. da Silva
Núcleo de Física Aplicada, Instituto de Física, Universidade de Brasília, Brasília, DF 70910-900, Brazil
e-mail: coaquira@unb.br

F. H. Aragón · J. A. H. Coaquira · S. W. da Silva
Instituto de Ciências Biológicas, Pós-graduação em Nanociência e Nanobiotecnologia, Universidade de Brasília, Brasília, DF 70910-900, Brazil

P. Hidalgo
Faculdade Gama-FGA, Setor Central Gama, Universidade de Brasília, Brasília, DF 72405-610, Brazil

R. Cohen · L. C. C. M. Nagamine
Instituto de Física, Universidade de São Paulo, São Paulo, SP 05508-090, Brazil

H. F. Brito
Instituto de Química, Universidade de São Paulo, São Paulo, SP 05508-000, Brazil

Introduction

Oxide semiconductors are interesting matrices for producing the so-called oxide-diluted magnetic semiconductor (ODMS) systems. These materials have drawn considerable attention due to their potential in

spintronic applications (Ohno 1998; Dietl et al. 2000). Therefore, a great deal of investigations has been devoted in recent years to obtain ODMS ferromagnetic compounds with a high Curie temperature (T_C). A room-temperature ferromagnetism (RTFM) has been reported for transition-metal (TM)-doped SnO_2 thin films and powders (Coey et al. 2004; Punnoose and Hays 2005; Fitzgerald et al. 2006). RTFM has been reported for Co-doped SnO_2 powders with Co concentrations below 1 mol%, but only a paramagnetic (PM) behavior has been observed for higher Co contents according to the authors (Punnoose et al. 2004; Hays et al. 2005).

On the other hand, it has been reported that the rare-earth (RE) dopant type strongly affect the magnetic properties of ODMS materials. RTFM properties were observed for the calcinated and sintered CeO_2 samples doped with Nd and Sm; whereas for the system with Gd, Tb, Er, and Dy dopants only a paramagnetic behavior was observed. Moreover, the synthesis method or technique seems to play a major role in the magnetism of these ODMS systems. ZnO:Er films synthesized by magnetron sputtering technique are reported to exhibit a coexistence of ferromagnetic and paramagnetic phases at room temperature (Qi et al. 2010). According to the authors, the strongest ferromagnetic signal has been observed for the 4.0 % Er-doped sample and that ferromagnetic contribution decreases with the increase of the Er content. In addition, other reports indicate that undoped and Gd-doped ZnO nanorods show RTFM properties (Panigrahy et al. 2011; Limaye et al. 2011). In other report, SnO_2:Gd nanomaterials synthesized by a co-precipitation method shows the absence of RTFM (Adhikari et al. 2010). Similarly, SnO_2:Er nanoparticles prepared by sol–gel method show only the occurrence of a paramagnetism with the presence of a weak Er–Er antiferromagnetic (AF) interactions, which become stronger as the Er concentration increases (Sambasivam et al. 2011). Recently, a strong paramagnetic-like behavior coexisting with a ferromagnetic order at room temperature has been determined for samples with Er content up to 5.0 %. Above this concentration, only a paramagnetic behavior has been determined.

In the last years, various mechanisms have been proposed to explain the observed RTFM properties. An indirect exchange via shallow donor electrons that form bound magnetic polarons (BMPs) (Coey et al. 2005; Jung et al. 2004; Qi et al. 2010; Aragón et al. 2013a), free carried-mediated coupling (Dietl et al. 2000) between magnetic cations, charge-transfer ferromagnetism (Coey et al. 2008), or a *F*-center exchange mechanism (Coey et al. 2004; Dimri et al. 2012) have been proposed to explain the ferromagnetism in ODMS systems. Besides, extrinsic origins to explain the RTFM such as impurity phases or metal segregates have also been reported in the literature (Punnoose et al. 2004; Duan et al. 2008; Sundaresan et al. 2006).

Despite the intense research, there are still controversies about the origin of the ferromagnetic properties observed in ODMS and its relation to the dopant type (3d or 4f). To the best of our knowledge, there are scarce reports about the magnetic properties of Gd doping of SnO_2 nanostructured system. In this work we presented a systematic study of the structural, magnetic, and hyperfine properties of Gd-doped SnO_2 nanoparticles synthesized by a polymer precursor method. Our results show that the Gd-doped SnO_2 nanoparticles form in the rutile-type structure when the Gd content is increased up to 10.0 %. It means that by the synthesis method used in this work, it is possible to overcome the solubility limit imposed by conventional methods.

Experimental details

SnO_2:Gd^{3+} nanoparticles with 1.0, 2.5, 5.0, 7.5, and 10.0 mol% of Gd have been synthesized by using a polymer precursor method reported as Pechini's method (Pechini 1967). The SnO_2:Gd^{3+} nanoparticles were obtained by using $SnCl_2{\cdot}H_2O$ and $Gd(NO_3)_3$ $5H_2O$ as the precursors. The amount of Gd was controlled by using the Gd/(Gd + Sn) ratio and the details of the synthesis are reported elsewhere (Aragón et al. 2010a, b; Gouvêa et al. 1996). The crystalline quality, structural parameters, and crystallite size were determined by the X-ray powder diffraction (XRD) technique using a commercial Rigaku diffractometer with Cu K_α radiation. The particle size has also been estimated from transmission electron microscopy (TEM) images. In order to confirm the nominal dopant concentration, an elemental analysis was done by Energy-dispersive X-ray spectroscopy (EDS) option of a scanning electron microscope (JEOL, model JSM 7001F). Magnetic measurements were carried out in the temperature interval from 2 up to 300 K and

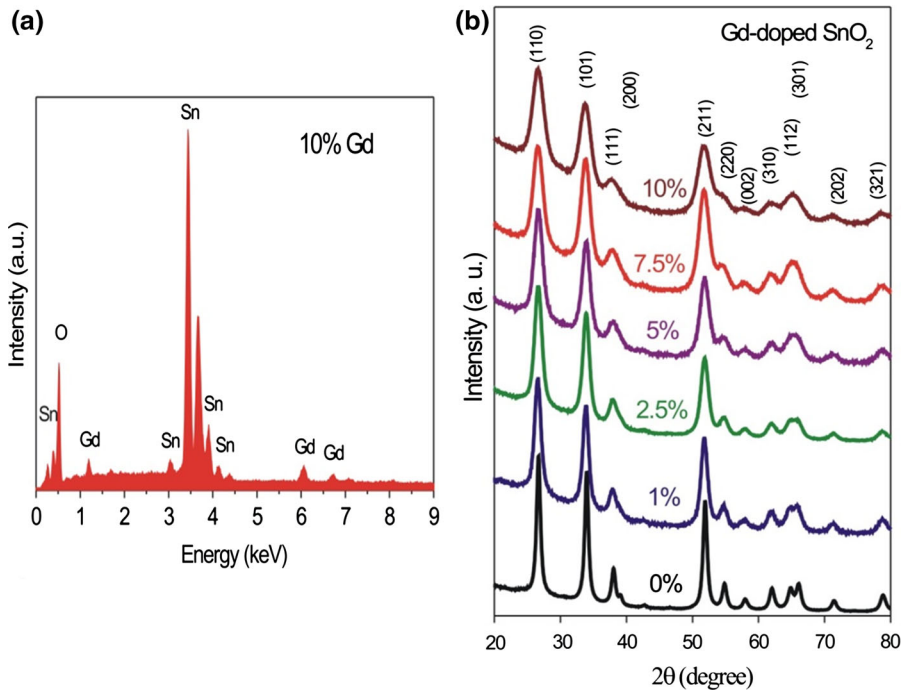

Fig. 1 **a** EDS spectrum obtained for the 10.0 % Gd-doped SnO_2 nanoparticles. **b** XRD patterns of the Gd-doped SnO_2 nanoparticles

applying magnetic fields up to 80 kOe using a Vibrating Sample Magnetometer unit of a physical property measurement system (PPMS, Quantum Design). Mössbauer spectra were recorded by using a conventional constant acceleration spectrometer with a $Ca^{119}SnO_3$ as the radioactive source. A natural Sn foil was used as the absorber for calibration. The analyses of the spectra have been carried out using a least-square fitting routine by using the Normos software and assuming a Lorentzian shape peaks.

Results and discussion

Structural analysis

In order to determine experimentally the gadolinium content in the SnO_2:Gd^{3+} nanoparticles EDS measurements were carried out. Figure 1a shows the EDS spectrum of the 10 mol% Gd-doped sample. Peaks located at around 1.2, 6.1, and 6.7 keV are assigned to the characteristic X-ray emissions of Gd^{3+} ions. In order to quantify the Gd content, several measurements have been done by considering different regions of the samples. Within the experimental uncertainties, the results shown in Table 1 confirm the nominal values of Gd content in the samples.

Figure 1b shows the XRD patterns of the SnO_2:-Gd^{3+}nanoparticles at room temperature. The XRD data analyses indicate the formation of the rutile-type phase (space group, P42/mnm) for all samples, and no evidence of additional crystalline or amorphous phases are found. The formation of only rutile-type phase has been corroborated by room-temperature Raman spectroscopy measurements (not shown here). The full width at half maximum (FWHM) of the diffraction peaks increases as the dopant concentration is increased (Fig. 1b). This effect can be attributed to the particle size reduction and/or to changes in the lattice strain extent (Karen and Woodward 1998). The X-ray diffraction patterns were further analyzed by the Rietveld refinement method by using the program General Structure Analyses System, (Larson and Von Dreele 1994). The parameters determined from the analyses are shown in Table 1. The mean crystallite size ($<D>$) was estimated assuming reflection peaks with Lorenzian shape and using the Scherrer relation: $<D> = K\lambda/L\cos\theta$, where $K = 0.9$ for spherical nanoparticles, λ is the wavelength (1.5418 Å for Cu K_α), L is the FWHM of the peaks, and θ is the diffraction angle. Since the Scherrer relation is valid just for the widening induced by the particle size reduction, no information of the lattice strain has been obtained. As observed in Table 1, $<D>$ shows a

Table 1 Parameters obtained from the Rietveld refinement of XRD data of SnO_2:Gd^{3+} nanoparticles

Gd (*x* %) (nominal)	Gd (*x* %) (EDS)	$\langle D \rangle_{XRD}$ (nm)	$\langle D \rangle_{TEM}$ (nm)	*a* (Å)	*c* (Å)	*c*/*a*	*u*	*V* (Å^3)
0.0[a]	–	14 ± 1	13.0	4.7359	3.1853	0.6726	0.299	71.44
1.0	1.1 ± 0.1	12 ± 1	11.5 ± 0.9	4.7386	3.1871	0.6726	0.312	71.56
2.5	2.8 ± 0.3	10 ± 1	–	4.7390	3.1914	0.6734	0.302	71.67
5.0	4.8 ± 0.3	8 ± 1	6.9 ± 0.9	4.7426	3.1953	0.6737	0.306	71.87
7.5	7.1 ± 0.2	5 ± 1	–	4.7429	3.1972	0.6741	0.311	71.92
10.0	10.4 ± 0.5	6 ± 1	5.1 ± 1.0	4.7403	3.2012	0.6753	0.324	71.93

u is the internal parameter of the rutile structure

[a] Data taken from Aragón (2013c)

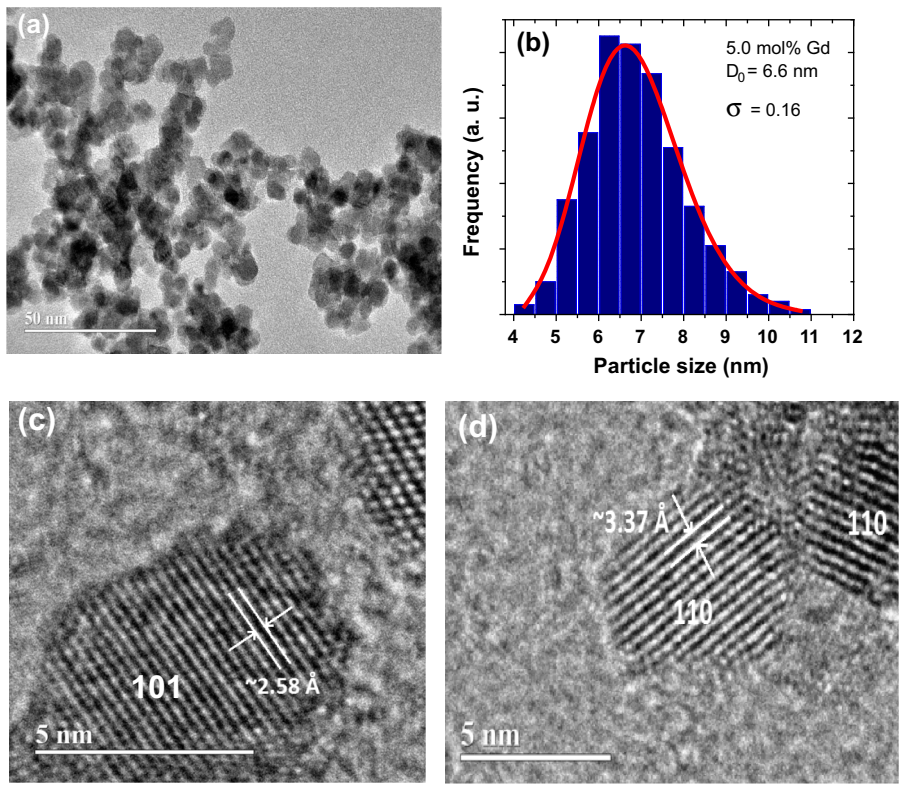

Fig. 2 **a** A TEM image of the SnO_2:Gd^{3+} nanoparticles doped with 5.0 mol% Gd. **b** The histogram distribution of the particles size, where the *solid line* represents the lognormal function. **c** High-resolution TEM images of the 5.0 and 10.0 mol% Gd-doped SnO_2 nanoparticles, respectively

decreasing tendency with the Gd content. Similar tendency has been reported for Fe-, Ni-, and Er-doped SnO_2 nanoparticles (Castro et al. 2005; Hidalgo et al. 2005; Aragón et al. 2013b). According to Castro et al. (2005), an excess of dopant ions segregates onto the surface of the particles and may lead to the reduction of the surface energy and, consequently, to the decrease of the final particle size. Although the segregation of Gd dopant at the particle surface cannot be excluded in the Gd-doped SnO_2 nanoparticles, we thought that the particle size reduction is induced just by the doping and the dopant amount enhances the size reduction. Currently, more studies are underway to clarify this issue and results will be published elsewhere.

Figure 2a shows one of the TEM image used to prepare the histogram distribution of the particle size for the 5.0 mol% Gd-doped sample. As observed in the inset, the histogram distribution is well modeled by a lognormal distribution. A mean particle size can be estimated by using the relation: $\langle D \rangle = D_0 \exp(\sigma^2/2)$, where D_0 is the median value and σ is the polydispersion parameter. A value of $\langle D \rangle = 6.9 \pm 0.9$ nm is obtained, which is in good agreement with the mean

crystalline size value determined from the XRD data analysis. Moreover, high-resolution TEM images shown in Fig. 2c, d for the 5.0 and 10.0 mol% Gd-doped samples confirm the formation of the rutile-type structure in our samples, and the particle sizes determined from the TEM images are in good agreement with those obtained from XRD experiments (see Table 1).

On the other hand, the *c*/*a* ratio shows a linear increase with the Gd content and suggests an asymmetric expansion of the unit cell with the increasing of Gd content. Moreover, the unit cell volume (V) shows a monotonous augmentation with the Gd content, although a reduction in the rate dV/dx (where x is the Gd content) is observed above 7.5 mol%. This behavior is opposite to that observed for Cr-doped SnO_2 nanoparticles (Aragón 2013) and suggests that the Gd^{3+} ions occupy mainly substitutional sites (Sn sites) in the SnO_2 matrix. Moreover, the large difference between 0.71 and 0.94 Å ionic radii of Sn^{4+} and Gd^{3+}, respectively, can explain the observed result. This is also in agreement with the theoretical study of defect and dopant states in SnO_2 matrix reported by Freeman and Catlow (1990). Those authors predicted, via energy formation calculations, the occurrence of substitutional dopant, and oxygen vacancy compensation in the SnO_2:Gd^{3+} system. An increasing tendency of unit cell volume as a function of Er content has been observed in SnO_2:Er^{3+} nanoparticles (Aragón et al. 2013b). The increasing tendency has been attributed to the substitution of Sn^{4+} by Er^{3+} in the SnO_2:Er^{3+} material. Although, the occupation of interstitial sites by the dopant ions is not excluded, the substitution of Sn by Gd ions seems to be the main regime in the lower Gd content region. The deviation from the linear behavior of V observed above 7.5 mol% could suggest that the Gd ions prefer to occupy interstitial sites for higher Gd-containing samples.

Magnetic properties

DC susceptibility (χ_{DC}) as a function of the temperature (T) was obtained in a field of $H = 5$ kOe for all samples (see Fig. 3). A typical paramagnetic behavior can be seen for all SnO_2:Gd^{3+} samples. The thermal dependence of the susceptibility could be well simulated by the Curie–Weiss law given by: $\chi_{DC} = \chi_0 + C/(T - \theta)$, where χ_0 represents any temperature-independent contribution, θ is the Curie–Weiss temperature, C is the Curie constant which is given by $C = N\mu_{eff}{}^2/3k_B$, N is the number of Gd^{3+} ions, μ_{eff} is their effective magnetic moment which is given by: $\mu_{eff} = 2\mu_B[J(J+1)]^{1/2}$, where J is the total angular momentum quantum number of gadolinium ions, and μ_B is the Bohr magneton.

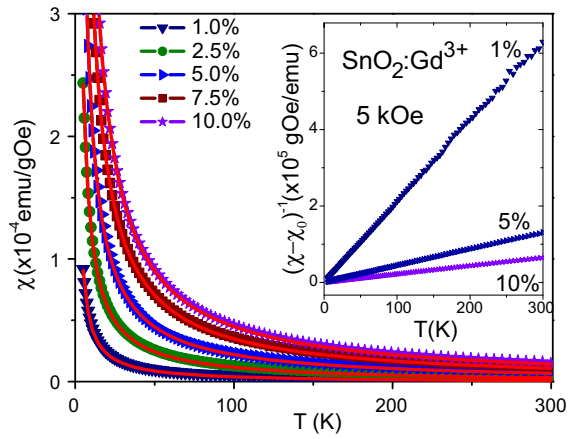

Fig. 3 Temperature (T) dependence of the DC susceptibility (χ_{DC}) of the SnO_2:Gd^{3+} nanoparticles. The *symbols* are the experimental data and the solid lines represent the fits to the Curie–Weiss law. In the *inset* is shown the linear dependence of the $(\chi - \chi_0)^{-1}$ on the temperature

Parameters obtained from these analyses are shown in Table 2. The Curie–Weiss temperature (θ) is rather small for all samples. The negative and small value of θ suggests that the Gd ions weakly interact antiferromagnetically. Moreover, the positive values of χ_0 could be related to any other contribution which shows a temperature-independent behavior.

As can be observed in Table 2, the Curie constant shows an increase with the Gd concentration. These C values are used to estimate the effective magnetic moment per Gd^{3+} ion μ_{eff}). By using the experimental μ_{eff} values and the theoretical one expected for free Gd^{3+} ion (7.94 μ_B), we are able to estimate the paramagnetic fraction of Gd ions (x_P). These values are also listed in Table 2 and they are slightly lower than the nominal content of Gd. The μ_{eff} does not show any decreasing tendency with the Gd content, which is in agreement with the weak antiferromagnetic interactions; otherwise, smaller effective moments would be expected for stronger antiferromagnetic interactions. Figure 3 shows the magnetization (M) as a function of the magnetic field (H) obtained at 300 K

Table 2 Parameters obtained from the fits of the susceptibility (χ_{DC}) versus temperature (T) curves using the modified Curie–Weiss law

Gd content (%)	χ_0 ($\times 10^{-5}$ emu/gOe)	C ($\times 10^{-5}$ emu K/gOe)	θ (K)	μ_{eff} (μ_B)	x_p (%)
1.0	4.4 ± 0.1	47 ± 1	−0.2 ± 0.1	7.57 ± 0.10	0.90
2.5	1.3 ± 0.1	128 ± 1	−0.2 ± 0.1	7.88 ± 0.08	2.46
5.0	4.2 ± 0.2	229 ± 1	−0.3 ± 0.1	7.48 ± 0.04	4.43
7.5	0.5 ± 0.4	362 ± 1	−0.5 ± 0.1	7.70 ± 0.02	7.05
10.0	2.9 ± 0.4	461 ± 1	−0.5 ± 0.1	7.55 ± 0.02	9.04

The error bars are obtained from the fit

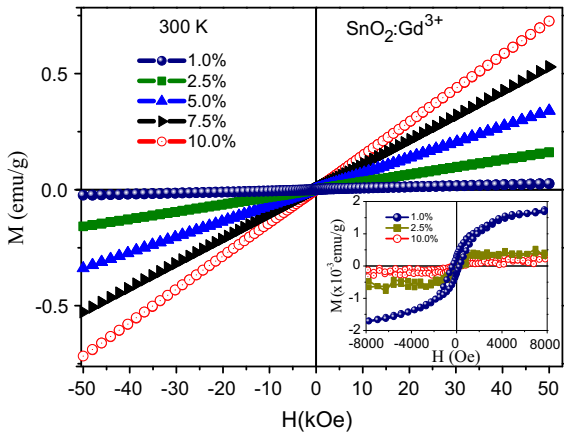

Fig. 4 Magnetization (M) versus applied magnetic field (H) curves obtained at 300 K for the SnO_2:Gd^{3+} nanoparticles. In the inset, we plotted the M versus H curves after subtracting the paramagnetic contribution

for all SnO_2:Gd^{3+} nanoparticles. A linear trend is determined in the high magnetic field region for all samples which has been assigned to the paramagnetic behavior. However, in the low-field region, a ferromagnetic contribution is determined. After subtracting the paramagnetic contribution, a saturation magnetization (M_S) of $\sim 2 \times 10^{-3}$ emu/g and a coercive field (H_C) of ~ 340 *Oe* have been determined for the 1.0 mol% Gd-doped sample. The ferromagnetic contribution becomes negligible as the Gd content is increased as can be observed in the inset of Fig. 4. A similar behavior has been determined for Er-doped SnO_2 nanoparticles in a previous work (Aragón et al. 2013a). The FM order was interpreted within the model proposed by Coey et al. (2005), in which model the ferromagnetism is mediated by shallow donor electrons that form bound magnetic polarons.

Although the charge-transfer ferromagnetism model proposed by Coey et al. (2008) could also explain the origin for the ferromagnetism observed for the 1.0 mol% Gd-doped sample, the effective magnetic moment values strongly suggest the presence of Gd ions in the valence state 3+ which is in agreement with the very stable half configuration of Gd ions ($4f^7$). Moreover, preliminary analysis of X-ray photoelectron spectroscopy (XPS) measurements (not shown here) corroborates the presence of only Gd^{3+} ions. On the other hand, other sources that explain the ferromagnetic contribution are associated with tin vacancies. It has been predicted via density functional theory calculations a ferromagnetic order in the undoped SnO_2 system containing tin vacancies (Rahman et al. 2008); nevertheless, the energy needed to generate this kind of defect is larger than that one to generate oxygen vacancies or interstitial tins (Kiliç and Zunger 2002) and we can exclude this possibility, at least for the low-doping region (Espinosa et al. 2011).

Figure 5 shows M versus H curves obtained at 5 K. As observed, only a paramagnetic behavior is determined for all samples in accordance with the Curie–Weiss behavior determined from χ_{DC} versus T curves. It means that the ferromagnetic contribution expected for the 1 mol% doped Gd sample is overwhelmed by the strong paramagnetic signal at low temperatures. M versus H curves are modeled using the Brillouin function given by: $M = M_S B(y)$ (Heiman et al. 1984), where M_S is the saturation magnetization, and y is given by $\mu_B JgH/k_B(T - T_o)$, where T_o is the phenomenological parameter that represents any magnetic interaction, and g is the Landé factor. Taking $g = 2$ and $J = 7/2$ for Gd^{3+} ions, good fits are obtained. As can be seen in Table 3, the magnetic saturation (M_S) exhibits an increasing tendency with the Gd content in the SnO_2 matrix. The interaction temperature (T_0) shows almost constant and negatives values suggesting that antiferromagnetic interactions occur in agreement with results obtained from the temperature

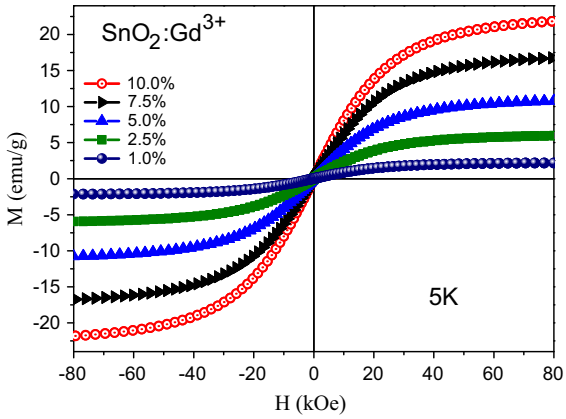

Fig. 5 Magnetization (M) versus applied magnetic field (H) obtained at 5 K for the SnO_2:Gd^{3+} nanoparticles

Table 3 Magnetic parameters obtained from the fit of M versus H curves measured at 5 K

Gd content (%)	M_S (emu/g)	T_0 (K)	x_S (%)
1.0	2.3 ± 0.1	−4.9 ± 0.1	0.88
2.5	6.2 ± 0.1	−5.2 ± 0.1	2.41
5.0	11.3 ± 0.1	−5.4 ± 0.1	4.40
7.5	17.5 ± 0.1	−5.6 ± 0.1	6.89
10.0	22.9 ± 0.1	−5.8 ± 0.1	9.06

M_S is the saturation magnetization, T_0 is the interaction temperature, and x_S is the Gd paramagnetic fraction

dependence of the DC susceptibility. Using the saturation magnetization values, the Gd^{3+} paramagnetic fraction (x_S) are estimated and values are listed in Table 3. Those values are in good agreement with those estimated from the thermal dependence of the DC susceptibility.

Hyperfine properties

In Fig. 6 are presented some room-temperature Mössbauer spectra of SnO_2:Gd^{3+} nanoparticles. A preliminary analysis indicates that the Mössbauer spectra are well resolved by fitting the experimental data with a doublet which represents an electric quadrupole splitting (QS). The linewidth (Γ) of the peaks for all samples is found to be larger ($\Gamma \sim 1.3$ mm/s for the 1.0 mol% Gd-doped samples), which is much larger than that expected for bulk SnO_2 and suggests the presence of a large number of

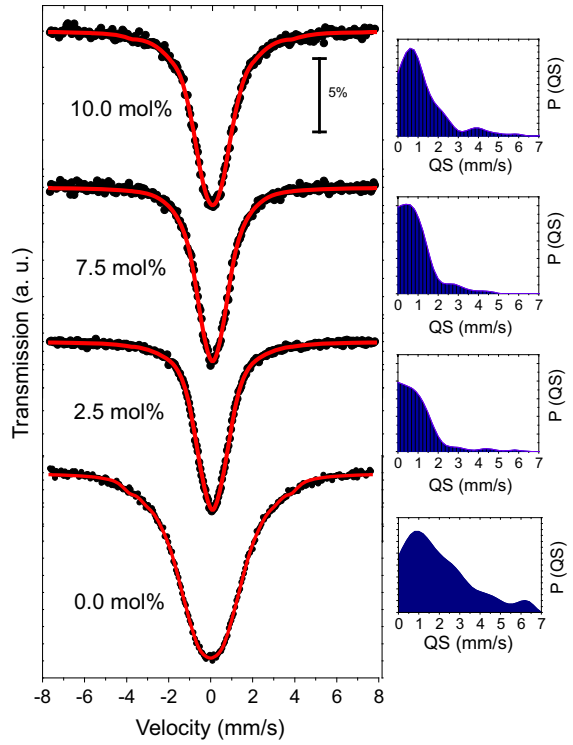

Fig. 6 Mössbauer spectra SnO_2:Gd^{3+} recorded at room temperature. The *symbols* are the experimental data and the lines represent the fits. The histogram distributions of the quadrupole splitting are shown at the *right panels*

doublets. In order to simulate the large number of doublets, the spectra were fitted by considering a distribution of QS's.

The obtained histograms of the distributions of QS are shown in Fig. 6. All spectra show an asymmetric maximum in the low-QS region. The presence of a distribution of QS's could be associated to the several non-equivalent surroundings of Sn^{4+} ions produced by the entrance of Gd^{3+} in the lattice. Moreover, preliminary analysis of XPS measurements suggests the presence of Sn–O bonds consistent with Sn^{2+} ions. This low valence state of Sn ions can provide a coordination that locally resembles the SnO phase (Kiliç and Zunger 2002; Togo et al. 2006). The presence of Sn^{2+} ions can provide a larger QS values which broaden the distribution of QS's, in special for the undoped SnO_2 nanoparticles. As observed in Fig. 6, the Gd doping largely reduces the distribution broadening. It suggests a drastic reduction in the population of Sn^{2+} ions likely due to the arising of complexes involving dopant ions and structural

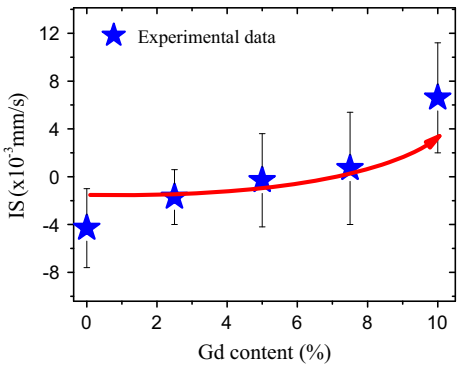

Fig. 7 Isomer shift (IS) as a function of the Gd^{3+} content in the SnO_2:Gd^{3+} nanoparticles. The *solid line* is drawn to guide the eyes

defects such as oxygen vacancies and/or interstitial cations. On the other hand, the isomer shift (IS) dependence on the Gd content is shown in Fig. 7. Due to the large error bars determined for the IS values, the IS seems nearly independent of the Gd content for samples with Gd content below 7.5 mol%. It means that the Gd doping does not provoke strong changes in the s-type electronic charge density visiting the Sn nuclei.

Conclusions

SnO_2:Gd^{3+} nanoparticles with rutile-type structure with Gd content from 1.0 to 10.0 mol% have been successfully synthesized by a polymer precursor method. The increase of the unit cell volume (V) suggests a substitutional solution of Gd ions in the SnO_2 matrix, although the presence of Gd ions in interstitial sites or the occurrence of segregation of Gd ions at particle surface must not be discarded. Magnetic measurements are consistent with the coexistence of paramagnetic and ferromagnetic phases for the low Gd content samples (up to 1.0 mol%) and this ferromagnetic phase can be attributed to the exchange interaction between Gd^{3+} ions mediated by the shallow donor electrons which form bound magnetic polarons. It is likely that above 1.0 mol% Gd content, the donor concentration is below the polaron percolation threshold and only a paramagnetic phase is observed. Room-temperature Mössbauer spectroscopy measurements reveal the occurrence of strong electric quadrupole interactions and no evidence of magnetic splitting are determined even for the 1.0 mol% Gd-doped sample. It seems that by controlling the donor concentration in this rare-earth doped SnO_2 compound one can enhance or favor the appearance of a ferromagnetic order of the magnetic moments.

Acknowledgments This work was financially supported by the Brazilian agencies CNPq, CAPES, FAP/DF, and FAPESP (proc. 2011/50556-0) Authors want to thank Dr. E. Guimarães for her help with the XRD experiments.

References

Adhikari R, Das AK, Karmakar D, Ghatak J (2010) Gd-doped SnO_2 nanoparticles: structure and magnetism. J Magn Magn Mater 322:3631–3637

Aragón FH (2013) Study of the origin of non-conventional magnetism in metal-doped SnO_2 nanoparticles. PhD. thesis, University of Brasilia, Brasília

Aragón FH, Coaquira JAH, Candela DS, Baggio Saitovitch E, Hidalgo P, Gouvêa D, Morais PC (2010a) Structural and hyperfine properties of Cr-doped SnO_2 nanoparticles. J Phys 217(012079):1–4

Aragón FH, Coaquira JAH, Hidalgo P, Brito SLM, Gouvêa D, Castro RHR (2010b) Structural and magnetic properties of pure and nickel doped SnO_2 nanoparticles. J Phys 22(496003):1–9

Aragón FH, Chitta VA, Coaquira JAH, Hidalgo P, Brito HF (2013a) Long-range ferromagnetic order induced by a donor impurity band exchange in SnO_2:Er^{3+} nanoparticles. J Appl Phys 114(203902):1–7

Aragón FH, Coaquira JAH, Hidalgo P, Cohen R, Nagamine LCCM, da Silva SW, Morais PC, Brito HF (2013b) Experimental evidences of substitutional solution of Er dopant in Er-doped SnO_2 nanoparticles. J Nanopart Res 15(1343):1–10

Castro RHR, Hidalgo P, Coaquira JAH, Bettini J, Zanchet D, Gouvêa D (2005) Surface segregation in SnO2–Fe2O3 nanopowders and effects in Mössbauer spectroscopy. Eur J Inorg Chem 11:2134–2138

Coey JMD, Douvalis AP, Fitzgerald CB, Venkatesan M (2004) Ferromagnetism in Fe-doped SnO_2 thin films. Appl Phys Lett 84:1332–1334

Coey JMD, Venkatesan M, Fitzgerald CB (2005) Donor impurity band exchange in diluted ferromagnetic oxides. Nat Mater 4:173–179

Coey JMD, Wongsaprom K, Alaria J, Venkatesan M (2008) Charge-transfer ferromagnetism in oxide nanoparticles. J Phys D 41:134012

Dietl T, Ohno H, Matsukura F, Cibert J, Ferrand D (2000) Zener model description of ferromagnetism in zinc-blende magnetic semiconductors. Science 287:1019–1022

Dimri MC, Khanduri H, Kooskora H, Subbi J, Heinmaa I, Mere A, Krustok J, Stern R (2012) Ferromagnetism in rare earth doped cerium oxide bulk samples. Phys Status Solidi A 209:353–358

Duan LB, Chu WG, Yu J, Wang YC, Zhang LN, Liu GY, Liang JK, Rao GH (2008) Structural and magnetic properties of

$Zn_{1-x}Co_xO$ ($0 < x \leq 0.30$). J Magn Magn Mater 320: 1573–1581

Espinosa A, Sánchez N, Sánchez-Marcos J, Andrés A, Muñoz C (2011) Origin of the magnetism in undoped and Mn-doped SnO2 thin films: Sn versus oxygen vacancies. J Phys Chem C 115:24054–24060

Fitzgerald CB, Venkatesan M, Dorneles LS, Gunning R, Stamenov P, Coey JMD, Stampe PA, Kennedy RJ, Moreira EC, Sias US (2006) Magnetism in dilute magnetic oxide thin films based on SnO_2. Phys Rev B 74(115307):1–10

Freeman and Catlow (1990) A computer modeling study of defect and dopant states in SnO_2. J Solid State Chem 85:65–75

Gouvêa D, Smith A, Bonnet JP (1996) Manganese segregation on the surface of SnO_2 based powders. Eur J Solid State Inorg Chem 33:1015–1023

Hays J, Punnoose A, Baldner R, Engelhard MH, Peloquin J, Reddy KM (2005) Relationship between the structural and magnetic properties of Co-doped SnO_2 nanoparticles. Phys Rev B 72:075203

Heiman D, Shapira Y, Foner S, Khazai B, Kershaw R, Dwight K, Wold A (1984) Exchange energy, magnetization, and Raman scattering of (Cd, Mn)Se. Phys Rev B 29:5634–5640

Hidalgo P, Castro RHR, Coelho ACV, Gouvêa D (2005) Surface segregation and consequent SO_2 sensor response in SnO_2–NiO. Chem Mater 17:4149–4153

Jung MGK, Park H, Jang HM, Ryu S, Kim YM (2004) Co-metal clustering as the origin of ferromagnetism in Co-doped ZnO thin films. Appl Phys Lett 84:1338–1340

Karen P, Woodward PM (1998) Liquid-mix disorder in crystalline solids: $ScMnO_3$. J Solid State Chem 141:78–88

Kiliç Ç, Zunger A (2002) Origins of coexistence of conductivity and transparency in SnO_2. Phys Rev Lett 88(095501):1–4

Larson AC, Von Dreele RB "GSAS: General Structural Analysis System" Los Alamos National Laboratory, Los Alamos NM (1994)

Limaye MV, Singh SB, Das R, Poddar P, Kulkarni K (2011) Room temperature ferromagnetism in undoped and Fe doped nanorods: microwave-ssisted synthesis. J Solid Stat Chem 184:391–400

Ohno H (1998) Making no magnetic semiconductor ferromagnetic. Science 281:951–956

Panigrahy B, Aslam M, Misra DS, Bahadur D (2011) Structural, optical and magnetic properties of Gd-doped ZnO nanorods by novel aqueous solution method. Int J Nanosci 10:629–633

Pechini M (1967) U.S. patent 3,330,697

Punnoose A, Hays J (2005) Possible metamagnetic origin of ferromagnetism in transition-metal-doped SnO_2. J Appl Phys 97: 10D321 1–3

Punnoose A, Hays J, Gopal V, Shutthanandan V (2004) Room-temperature ferromagnetism in chemically synthesized $Sn_{1-x}Co_xO_2$ powders. Appl Phys Lett 85:1559–1561

Qi J, Gao D, Liu J, Yang W, Wang Q, Zhou J, Yang Y, Liu J (2010) Magnetic properties of Er-doped ZnO films prepared by reactive magnetron sputtering. Appl Phys A 100:79–82

Rahman G, García-Suárez VM, Hong SC (2008) Vacancy-induced magnetism in SnO_2: a density functional study. Phys Rev B 78:184404 1–184404 5

Sambasivam S, Joseph D, Jeong J, Choi B, Lim K, Kim S, Song T (2011) Antiferromagnetic interactions in Er-doped SnO_2 DMS nanoparticles. J Nanopart Res 13:4623–4630

Sundaresan A, Bhargavi R, Rangarajan N, Siddesh U, Rao CNR (2006) Ferromagnetism as a universal feature of nanoparticles of the otherwise nonmagnetic oxides. Phys Rev B 74(161306):1–4

Togo A, Oba F, Tanaka I, Tatsumi K (2006) First-principles calculations of native defects in tin monoxide. Phys Rev B 74(195128):1–8